

Dynamics of quantum double dark-solitons and an exact finite-size scaling of Bose-Einstein condensation

Kayo Kinjo¹, Jun Sato² and Tetsuo Deguchi³

¹ Department of Physics, Center for Soft Matter Physics, Ochanomizu University, Bunkyo-ku, Tokyo 112-8610, Japan

² Faculty of Engineering, Tokyo Polytechnic University, Atsugi 243-0297, Japan

³ Department of Physics, Faculty of Core Research, Ochanomizu University, Bunkyo-ku, Tokyo 112-8610, Japan

E-mail: deguchi@phys.ocha.ac.jp

June 2022

Abstract. We show several novel aspects in the exact non-equilibrium dynamics of quantum double dark-soliton states in the Lieb-Liniger model for the one-dimensional Bose gas with repulsive interactions. We also show an exact finite-size scaling of the fraction of the Bose-Einstein condensation (BEC) in the ground state, which should characterize the quasi-BEC in quantum double dark-soliton states that we assume to occur in the weak coupling regime. First, we show the exact time evolution of the density profile in the quantum state associated with a quantum double dark-soliton by the Bethe ansatz. Secondly, we derive a kind of macroscopic quantum wave-function effectively by exactly evaluating the square amplitude and phase profiles of the matrix element of the field operator between the quantum double dark-soliton states. The profiles are close to those of dark-solitons particularly in the weak-coupling regime. Then, the scattering of two notches in the quantum double dark-soliton state is exactly demonstrated. It is suggested from the above observations that the quasi-BEC should play a significant role in the dynamics of quantum double dark-soliton states. If the condensate fraction is close to 1, the quantum state should be well approximated by the quasi-BEC state where the mean-field picture is valid.

Keywords: quantum dynamics, dark-soliton, BEC, finite-size scaling

Submitted to: *J. Phys. A: Math. Gen.*

1. Introduction

The experimental realization of trapped atomic gases in one dimension (1D) has provided a new motivation for the study of strong correlations in fundamental quantum

mechanical systems of interacting particles [1, 2, 3, 4, 5]. Furthermore, the non-equilibrium dynamics of closed interacting quantum systems is now extensively studied in 1D by experiments and theories [6, 7, 8]. In many 1D quantum interacting systems quantum fluctuations may play a key role and often lead to subtle nontrivial effects. We thus expect that fundamental many-body properties such as the quasi-Bose-Einstein condensation (BEC) should play a key role in the nontrivial quantum dynamics such as quantum dark-solitons.

Let us introduce a theoretical model for the 1D system of interacting bosons with repulsive short-range potentials. Here we call it the 1D Bose gas. For simplicity we assume that the interactions are given by the delta-function potentials, since they give nontrivial effects in the 1D case although they are simple. For instance, the scattering length depends on the strength of the delta-function potential in 1D systems. We thus have the Lieb-Liniger model (LL model) as the system of the 1D Bose gas. The Hamiltonian of the LL model is given by [9, 10]:

$$\mathcal{H}_{\text{LL}} = - \sum_{j=1}^N \frac{\partial^2}{\partial x_j^2} + 2c \sum_{j < k}^N \delta(x_j - x_k). \quad (1)$$

Here we assume the periodic boundary conditions of the system size L on the wave-functions. We employ a system of units with $2m = \hbar = 1$, where m denotes the mass of the particle. We recall that the coupling constant c is positive. It is an exactly solvable model of the 1D quantum many-body system. It is known that all the eigenvectors are constructed by the Bethe-ansatz method. Furthermore, the Gross-Pitaevskii (GP) equation appears as the Heisenberg equation of motion for the second-quantized Hamiltonian of the LL model. It is expressed in terms of the classical complex scalar field ψ as follows [11].

$$i \frac{\partial}{\partial t} \psi = - \frac{\partial^2}{\partial x^2} \psi + 2c|\psi|^2 \psi - \mu \psi. \quad (2)$$

We expect that the GP equation should play a central role in the long-distance mean-field behavior of the 1D Bose gas in some quantum state if the quasi-BEC occurs in the quantum state of the LL model especially in the weak-coupling regime. If it is the case, the solution of the GP equation should correspond to the macroscopic wave-function of the quasi-BEC state, and describe the quantum state well at least approximately.

Thus, if the BEC occurs in some quantum states of the LL model, we expect that the GP equation should play a central role for characterizing the quantum state, although it is only a partial differential equation for a complex scalar variable. In the present research, we assume that the quasi-BEC should occur if the coupling constant is small enough with respect to the system size or the number of bosons, and hence some solutions of the GP equation such as multiple dark-solitons can be compared with the density profiles of some quantum states in the quasi BEC of the 1D Bose gas. In fact, we shall show a finite-size scaling of the quasi BEC in the present research.

It should be remarked that such quantum states whose density profiles coincide with those of single dark-solitons of the GP equation have been constructed explicitly

in the form of superposition of the yrast states in the Lieb-Liniger model [12]. The construction resolved a long standing problem suggested by Ishikawa and Takayama almost forty years ago [13]. Furthermore, several significant properties in the non-equilibrium dynamics of a quantum single dark-soliton have been exactly investigated [14] and the ideal Gaussian weights have been introduced [15, 16]. Moreover, the phase shift has numerically been estimated in the scattering of two quantum dark-solitons [17].

There is another aspect of quantum dark-soliton states. Successive measurements of particle positions in the Lieb-Liniger model also leads to observing quantum dark-solitons numerically [18, 19]. There is a question how the density profile of a superposition of yrast states is related to the successive measurements of particle positions. When the coupling constant c is equal to zero it was analytically shown that the construction of the quantum dark-soliton state with the Gaussian weight [15] is related to the particle position method [18] in Ref. [15]. When the coupling constant is small and nonzero: $c > 0$, an ansatz was proposed to bridge between the calculation of single-particle density and the particle position method [20].

In the present paper we show various novel aspects in the exact non-equilibrium dynamics of quantum double dark-solitons, which give pairs of notches in the density profiles, by explicitly constructing corresponding quantum states in the Lieb-Liniger model of the 1D Bose gas with the repulsive interactions. We also show an exact finite-size scaling of the fraction of the BEC in the ground state. It should characterize the quasi-BEC which we assume to occur in quantum double dark-soliton states in the weak coupling regime. We show that if the coupling constant decreases as a power of the system size, condensate fraction does not vanish and remains constant when we send the system size to a very large value with fixed density. If condensate fraction is nonzero for a large number of particles, we call it BEC according to the Penrose-Onsager criterion. It follows from it that the quasi-BEC occurs only if the coupling constant is very small with respect to the system size. Therefore quantum states of dark-solitons may appear particularly in the weak coupling regime.

Based on the definition of the quasi-BEC we derive a kind of macroscopic quantum wave-function by exactly deriving the amplitude and phase profiles of the matrix element of the bosonic field operator, by making use of Slavnov's formula of form factors. Here we recall that the bosonic field operator is defined in the second-quantized Hamiltonian of the Lieb-Liniger model.

Let us briefly summarize the finite-size scaling of the quasi-BEC. The scaling behavior of the quasi-BEC in the 1D Bose gas is fundamental when we send particle number N or system size L to very large values. We define interaction parameter γ by $\gamma = c/n$ with coupling constant c in the delta-function potentials and density $n = N/L$. We show that if γ is given by a negative power of N , i.e. $\gamma = A/N^\eta$, condensate fraction n_0 is nonzero and constant for any large value of L or N . We also show that exponent η and amplitude A are independent of density n , and evaluate them as functions of n_0 . Condensate fraction n_0 is thus given by a scaling function of variable γN^η . If the condensate fraction of a quantum state with large N is nonzero in the 1D Bose gas, we

suggest that the classical mean-field approximation such as the GP equation is valid for the state [21]. Furthermore, we show that the 1D Bose gas of a finite particle number may have the same condensate fraction for any large L .

Finally, we mention some potentially relevant results in the following. For strong and intermediate interaction strengths, the Lieb-Liniger Gross-Pitaevski equation is introduced, which is an extension of the GP equation [22]. Associated with the quantum states of dark solitons, bound states of dark solitons are numerically studied by solving the GP equation [23], dynamics of a bright soliton in quasi-BEC with time-dependent atomic scattering length in an repulsive parabolic potential [24], quantized quasi-two-dimensional Bose-Einstein condensates with spatially modulated nonlinearity [25], matter rogue wave in Bose-Einstein condensates with attractive atomic interaction [26], exact soliton solutions, and nonlinear modulation instability in spinor Bose-Einstein condensates [27].

The contents of the paper consist of the following. In §2 we explain the Bethe ansatz and useful formulas for evaluating the form factors of the field operator. We also define the winding number for solutions of the GP equation under the periodic boundary conditions. In §3 we show the time evolution of the quantum double dark-soliton state constructed with equal weight for the following two cases: (i) The soliton positions X_1 and X_2 are different: $X_1 = L/4$ and $X_2 = 3L/4$; (ii) the soliton positions are same: $X_1 = X_2 = 0$. We also show the time evolution of the quantum double dark-soliton state constructed with the Gaussian weights. Here, two notches have different speeds, and we evaluate the phase shift in the collision of the two dark solitons. In §4 we show the finite-size scaling behavior of condensate fraction in the 1D Bose gas with repulsive interactions at zero temperature. According to it, the fraction of the quasi-BEC condensate is equal to 0.99 for the quantum double dark-soliton state with $N = L = 20$ and $c = 0.05$ studied in the present research.

2. Method

2.1. Bethe ansatz equations

In the LL model, the Bethe ansatz offers an exact eigenstate with an exact energy eigenvalue for a given set of quasi-momenta k_1, k_2, \dots, k_N satisfying the Bethe ansatz equations (BAE) for $j = 1, 2, \dots, N$:

$$k_j L = 2\pi I_j - 2 \sum_{\ell \neq j}^N \arctan \left(\frac{k_j - k_\ell}{c} \right). \quad (3)$$

Here I_j 's are integers for odd N and half-odd integers for even N . We call them the Bethe quantum numbers. The total momentum P and the energy eigenvalue E are expressed in terms of the quasi-momenta as

$$P = \sum_{j=1}^N k_j = \frac{2\pi}{L} \sum_{j=1}^N I_j, \quad E = \sum_{j=1}^N k_j^2. \quad (4)$$

If we specify a set of Bethe quantum numbers $I_1 < \dots < I_N$, BAE in Equation (3) have a unique real solution $k_1 < \dots < k_N$ [28, 29]. In particular, the sequence of the Bethe quantum numbers of the ground state is given by

$$I_j = -(N+1)/2 + j \quad \text{for } j \in \mathbb{Z} \text{ with } 1 \leq j \leq N. \quad (5)$$

The Bethe quantum numbers for low lying excitations are systematically derived by putting holes or particles in the perfectly regular ground-state sequence.

2.2. Coupling constant

In the thermodynamic limit several physical quantities of the LL model are characterized by the single parameter $\gamma = c/n$, where $n = N/L$ is the density of particle number N . We often fix the particle-number density as $n = 1$ throughout the present paper, and change coupling constant c so that we have different values of γ .

2.3. Quantum double dark-soliton state

A quantum state possessing the two notches in both its density profile and square amplitude was proposed in [30]. Such quantum state is called the quantum double dark-soliton state given by the superposition of “two-hole” excitation states

$$|X_1, X_2, N\rangle := \frac{1}{\sqrt{\mathcal{M}}} \sum_{p \in \mathbf{P}} e^{i(p_1 X_1 + p_2 X_2)} |p_1, p_2, N\rangle \quad (6)$$

with a normalization factor \mathcal{M} . Here $|p_1, p_2, N\rangle$ denotes a two-hole excitation for which the configuration of the Bethe quantum numbers are determined by the two holes p_1 and p_2 , and \mathbf{P} denotes the set of all allowed pairs of two holes. Figure 1 illustrates how to punch the holes in the series of the Bethe quantum numbers. The density profile of this state $\langle X_1, X_2, N | \hat{\psi}^\dagger(x) \hat{\psi}(x) | X_1, X_2, N \rangle$ shows the two density notches at the positions $X = X_1, X_2$, which coincides with the squared amplitude of the elliptic soliton [30]. Here, by the determinant formula for the norms of Bethe eigenstates [31, 32] we can effectively evaluate the matrix element

$$\begin{aligned} & \langle X_1, X_2, N | \hat{\psi}^\dagger(x) \hat{\psi}(x) | X_1, X_2, N \rangle \\ &= \frac{1}{N} \sum_p \exp \left[2\pi i(p - p') \frac{(x - X)}{L} \right] \langle p'_1, p'_2, N | \hat{\psi}^\dagger(0) \hat{\psi}(0) | p_1, p_2, N \rangle \end{aligned} \quad (7)$$

and that of the form factors of the density operator [33, 34, 35]

$$\begin{aligned} & \langle p'_1, p'_2, N | \hat{\psi}^\dagger(0) \hat{\psi}(0) | p_1, p_2, N \rangle \\ &= (-1)^{N(N+1)/2} (P - P') \left(\prod_{j,\ell=1}^N \frac{1}{k'_j - k_\ell} \right) \left(\prod_{j>\ell}^N k_{j,\ell} k'_{j,\ell} \sqrt{\frac{\hat{K}(k'_{j,\ell})}{\hat{K}(k_{j,\ell})}} \right) \\ & \quad \times \frac{\det U(k, k')}{\sqrt{\det G(k) \det G(k')}}, \end{aligned} \quad (8)$$

where the quasimomenta $\{k_1, \dots, k_N\}$ and $\{k'_1, \dots, k'_N\}$ give the eigenstates $|P\rangle$ and $|P'\rangle$, respectively. We use the abbreviations $k_{j,\ell} := k_j - k_\ell$ and $k'_{j,\ell} := k'_j - k'_\ell$. The

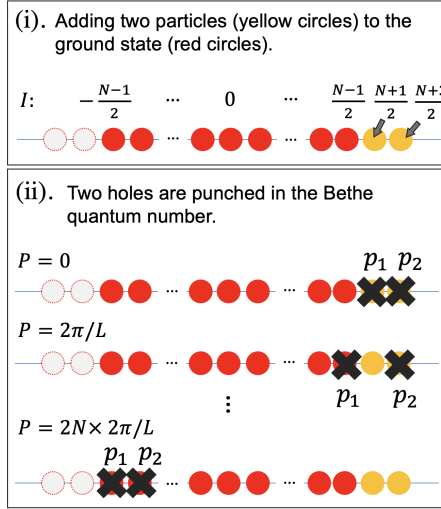


Figure 1. (Color online) Configuration of the Bethe quantum numbers for a quantum double dark-soliton state. (i) Configuration derived by adding two particles (yellow circles) to that of the ground state (red circles). (ii) A series of configurations derived by punching two holes, which correspond to $\mathbf{p} = \{p_1, p_2\}$, in the configuration of the Bethe quantum numbers constructed in panel (i). Reproduced from [30].

kernel $\hat{K}(k)$ is defined by $\hat{K}(k) = 2c/(k^2 + c^2)$. The matrix $G(k)$ is called the Gaudin matrix, whose (j, ℓ) th element is given by

$$G(k)_{j,\ell} = \delta_{j,\ell} \left[L + \sum_{m=1}^N \hat{K}(k_{j,m}) \right] - \hat{K}(k_{j,\ell}) \quad \text{for } j, \ell = 1, 2, \dots, N. \quad (9)$$

The matrix elements of the $(N-1)$ by $(N-1)$ matrix $U(k, k')$ are given by

$$U(k, k')_{j,\ell} = 2\delta_{j\ell} \text{Im} \left[\prod_{a=1}^N \frac{k'_a - k_j + ic}{k_a - k_j + ic} \right] + \frac{\prod_{a=1}^N (k'_a - k_j)}{\prod_{a \neq j}^N (k_a - k_j)} \left(\hat{K}(k_{j,\ell}) - \hat{K}(k_{N,\ell}) \right). \quad (10)$$

We can also consider the matrix element of the single field operator

$$\begin{aligned} & \langle X', N-1 | \hat{\psi}(x) | X, N \rangle \\ &= \frac{1}{\sqrt{N(N-1)}} \sum_{p=0}^N \sum_{p'=0}^{N-1} \exp \left[2\pi i (p - p') \frac{x}{L} \right] \exp \left[-2\pi i \left(\frac{pq}{N} - \frac{p'q'}{N} \right) \right] \\ & \times \langle P', N-1 | \hat{\psi}(0) | P, N \rangle, \end{aligned} \quad (11)$$

where $P = 2\pi p/L$ and $P' = 2\pi p'/L$ denote the total momenta of the normalized Bethe eigenstates in the type II branch $|P, N\rangle$ and $|P', N\rangle$, respectively. The determinant formula is given by [31, 32, 33, 36, 34, 35]

$$\langle P', N-1 | \hat{\psi}(0) | P, N \rangle = (-1)^{N(N+1)/2+1} \left(\prod_{j=1}^{N-1} \prod_{\ell=1}^N \frac{1}{k'_j - k_\ell} \right) \left(\prod_{j>\ell}^N k_{j,\ell} \sqrt{k_{j,\ell}^2 + c^2} \right)$$

$$\times \left(\prod_{j>\ell}^{N-1} \frac{k'_{j,\ell}}{\sqrt{(k'_{j,\ell})^2 + c^2}} \right) \frac{\det \widehat{U}(k, k')}{\sqrt{\det G(k) \det G(k')}}, \quad (12)$$

where the quasi-momenta $\{k_1, \dots, k_N\}$ and $\{k'_1, \dots, k'_{N-1}\}$ give the eigenstates $|P, N\rangle$ and $|P', N-1\rangle$, respectively. Here we remark that the symbol X' corresponds to an integer q' . We recall that the matrix $G(k)$ denotes the Gaudin matrix, whose (j, ℓ) th element is given in (9). The matrix elements of the $(N-1)$ by $(N-1)$ matrix $\widehat{U}(k, k')$ are given by

$$\begin{aligned} \widehat{U}(k, k')_{j,\ell} = & 2\delta_{j\ell} \text{Im} \left[\frac{\prod_{a=1}^{N-1} (k'_a - k_j + ic)}{\prod_{a=1}^N (k_a - k_j + ic)} \right] \\ & + \frac{\prod_{a=1}^{N-1} (k'_a - k_j)}{\prod_{a \neq j}^N (k_a - k_j)} \left(\hat{K}(k_{j,\ell}) - \hat{K}(k_{N,\ell}) \right). \end{aligned} \quad (13)$$

2.4. One-particle reduced density matrix

The matrix element of the one-particle reduced density matrix, $\rho_1(x, y) := \langle x | \hat{\rho}_1 | y \rangle$, for a quantum system is expressed as a correlation function in the ground state $|\lambda\rangle$:

$$\rho_1(x, y) = \langle \lambda | \hat{\psi}^\dagger(y) \hat{\psi}(x) | \lambda \rangle. \quad (14)$$

In the LL model we can numerically evaluate the correlation function by the form factor expansion. Inserting the complete system of eigenstates, $\sum_\mu |\mu\rangle \langle \mu|$, we have

$$\rho_1(x, y) = \sum_\mu e^{i(P_\mu - P_\lambda)(y-x)} |\langle \mu | \hat{\psi}(0) | \lambda \rangle|^2, \quad (15)$$

where P_μ denote the momentum eigenvalues of eigenstates $|\mu\rangle$. Each form factor in the sum (15) is expressed as a product of determinants by making use of the determinant formula for the norms of Bethe eigenstates [31] and that for the form factors of the field operator [33, 35, 34]:

$$\begin{aligned} \langle \mu | \hat{\psi}(0) | \lambda \rangle = & (-1)^{N(N+1)/2+1} \left(\prod_{j=1}^{N-1} \prod_{\ell=1}^N \frac{1}{k'_j - k_\ell} \right) \left(\prod_{j>\ell}^N k_{j,\ell} \sqrt{k_{j,\ell}^2 + c^2} \right) \\ & \times \left(\prod_{j>\ell}^{N-1} \frac{k'_{j,\ell}}{\sqrt{(k'_{j,\ell})^2 + c^2}} \right) \frac{\det U(k, k')}{\sqrt{\det G(k) \det G(k')}}, \end{aligned} \quad (16)$$

where the quasi-momenta $\{k_1, \dots, k_N\}$ and $\{k'_1, \dots, k'_{N-1}\}$ give the eigenstates $|\lambda\rangle$ and $|\mu\rangle$, respectively. Here we have employed the abbreviated symbols $k_{j,\ell} := k_j - k_\ell$ and $k'_{j,\ell} := k'_j - k'_\ell$. The matrix $G(k)$ is the Gaudin matrix, whose (j, ℓ) th element is $G(k)_{j,\ell} = \delta_{j,\ell} \left[L + \sum_{m=1}^N K(k_{j,m}) \right] - K(k_{j,\ell})$ for $j, \ell = 1, 2, \dots, N$, where the kernel $K(k)$ is defined by $K(k) = 2c/(k^2 + c^2)$. The matrix elements of the $(N-1)$ by $(N-1)$ matrix $U(k, k')$ are given by [34, 33, 35, 31]

$$U(k, k')_{j,\ell} = 2\delta_{j\ell} \text{Im} \left[\frac{\prod_{a=1}^{N-1} (k'_a - k_j + ic)}{\prod_{a=1}^N (k_a - k_j + ic)} \right]$$

$$+ \frac{\prod_{a=1}^{N-1} (k'_a - k_j)}{\prod_{a \neq j}^N (k_a - k_j)} (K(k_{j,\ell}) - K(k_{N,\ell})). \quad (17)$$

2.5. Winding number

We introduce the winding number J associated with solutions of the GP equation under the periodic boundary conditions. Let us assume that a solution of the GP equation $\phi(x) = \sqrt{\rho(z)} \exp[i\varphi(x)]$ satisfies the periodic boundary conditions:

$$\varphi(x + L) = \varphi(x) + 2\pi J \quad (18)$$

where J is an arbitrary integer. The integer J is called the winding number [37, 38]. In the previous study, we constructed the quantum single dark-soliton with a nonzero-winding number.

3. Dynamics of quantum double dark-soliton

3.1. Time evolution of quantum double dark-soliton state constructed with equal weight

By applying the time dependent field operator $\hat{\psi}(x, t)$, the density profile and the matrix element of the quantum state evolve in time as follows.

$$\begin{aligned} \rho_Q(x, t) : &= \langle X_1, X_2, N | \hat{\rho}(x, t) | X_1, X_2, N \rangle \\ &= \frac{1}{\mathcal{M}} \sum_{\mathbf{p}, \mathbf{p}' \in \mathbf{P}} e^{i(P-P')x} e^{i(p_1 X_1 + p_2 X_2)} e^{-i(p'_1 X_1 + p'_2 X_2)} e^{-i(E-E')t} \\ &\quad \times \langle p'_1, p'_2, N | \hat{\rho}(0, 0) | p_1, p_2, N \rangle, \end{aligned} \quad (19)$$

$$\begin{aligned} \psi_Q(x, t) : &= \langle X_1, X_2, N - 1 | \hat{\psi}(x, t) | X_1, X_2, N \rangle \\ &= \frac{1}{\sqrt{\mathcal{M}_{N-1} \mathcal{M}_N}} \sum_{\mathbf{p}, \mathbf{p}' \in \mathbf{P}} e^{i(P-P')x} e^{-i(E-E')t} e^{i(p_1 X_1 + p_2 X_2)} e^{-i(p'_1 X_1 + p'_2 X_2)} \\ &\quad \times \langle p'_1, p'_2, N - 1 | \hat{\psi}(0, 0) | p_1, p_2, N \rangle, \end{aligned} \quad (20)$$

where E is the energy of the state $|p_1, p_2, N\rangle$, and $\hat{\rho}(x, t) = \hat{\psi}^\dagger(x, t) \hat{\psi}(x, t)$. We have obtained the exact expressions of the time evolution in Equations (19) and (20) since the Bethe Ansatz method gives the exact energy for the quantum state $|X_1, X_2, N\rangle$.

3.1.1. Quantum dark-soliton positions located at $X_1 = L/4$ and $X_2 = 3L/4$ initially
Figure 2 shows the time evolution of the density profile $\rho_Q(x, t)$ with soliton positions $X_1 = \frac{L}{4}$ and $X_2 = \frac{3L}{4}$ at $t = 0$ under the periodic boundary conditions. Note that the density profile shown in panel (a) of Figure 2 is identical to the upper-left panel of Figure 9 for $c = 0.05$ in Ref. [30]. Thus, at $t = 0$, the density profile of the quantum double dark-soliton coincides with that of the elliptic soliton solution of the GP equation. The positions of the notches are plotted in the areas of the darker color in Figure 2 in the left panel. The notches evolve in time in parallel in the plots of the left panel of Figure 2, while the soliton notches are filled progressively as shown in panels (a), (b), (c), and

(d) of Figure 2. Though the widths of the notches become wider in time evolution, the distance between the bottoms of the notches is constant through the time evolution. For example, at $t = 11$, the notches are located at $x_1 = 1.9115$ and $x_2 = 11.9115$, and the distance between the two notches is given by $\Delta x = x_1 - x_2 = 10 = L/2$, which is the same as that of $t = 0$.

Figure 3 shows the evolution of the square amplitude of the matrix element $|\psi_Q(x, t)|^2$ with soliton positions $X_1 = \frac{L}{4}$ and $X_2 = \frac{3L}{4}$ at $t = 0$ under the periodic boundary conditions. The average density is decreasing in the time evolution of the square amplitude $|\psi_Q(x, t)|^2$ in Figure 3, while the notches in Figure 2 are being filled gradually as time t increases. We suggest that the main components of which the quantum soliton state consists should decrease with in the case of the square amplitude, whereas the density is conserved as a whole for any t : $\int_0^L dx \rho_Q(x, t) = N$.

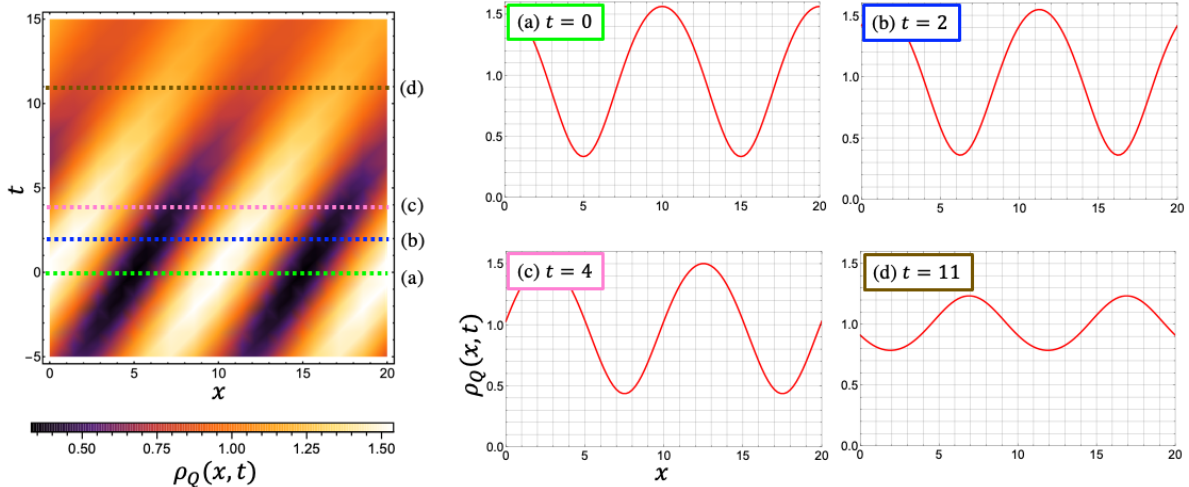


Figure 2. (Color online) Time evolution of the density profile $\rho_Q(x, t)$ (left panel) and its snapshots at $t = 0, 2, 4, 11$, in panels (a), (b), (c), and (d), respectively, for $N = L = 20$, $X_1 = \frac{L}{4}$, $X_2 = \frac{3L}{4}$, and $c = 0.05$. In the left panel, the vertical axis corresponds to time, and the horizontal one to the x coordinate. Panel (a) shows the density profile at $t = 0$, which corresponds to the green dotted line in the left panel of the density plot. Panels (b), (c), and (d) show the density profile at $t = 2, 4, 11$, which correspond to the blue, pink, and ochre dotted lines in the left panel of the density plot, respectively. The frames of the legends of panels (a), (b), (c), and (d) correspond to the green, blue, pink, and ochre colors, respectively.

In the same way as the density profile, the trajectories of the notches are shown with the lines in darker color in the left panel of Figure 3. We observed that the values at the bottoms of the notches are almost zero constantly in panels (a), (b), (c), and (d) of Figure 3. Consequently, Figure 3 shows the notches in the contour plot more clearly than Figure 2.

The time evolution of the phase profile is shown in Figure 4. Here we remark that the phase is given by the argument of the matrix element of Equation (20). The abrupt jumps are located at the positions of the notches in Figure 3. The abrupt jumps move

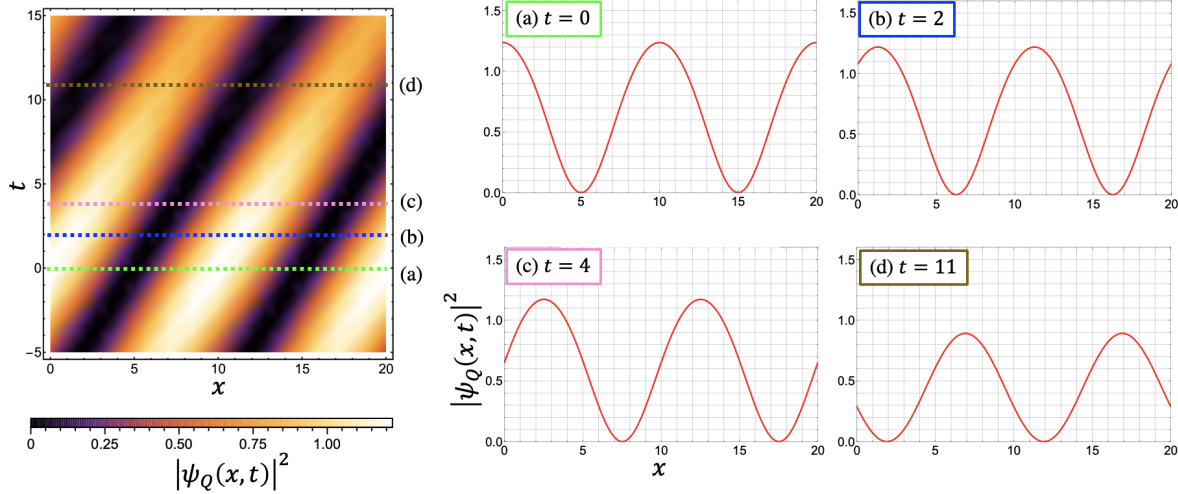


Figure 3. (Color online) Time evolution of the square amplitude of the matrix elements $\psi_Q(x, t)$ (left panel) and its snapshots at $t = 0, 2, 4, 11$ (right panel) for $N = L = 20$, $X_1 = \frac{L}{4}$, $X_2 = \frac{3L}{4}$, and $c = 0.05$. Panel (a) shows the density profile at $t = 0$, which corresponds to the green dotted line in the left panel of the density plot. Panels (b), (c), and (d) shows the density profile at $t = 2, 4, 11$, which correspond to the blue, pink, and ochre dotted lines in the left panel of the density plot, respectively. The frames of the legends of panels (a), (b), (c), and (d) correspond to the green, blue, pink, and ochre colors, respectively.

with the same constant speed as the square amplitude profile. The whole phase profiles are shifted toward the negative direction in the time evolution. Moreover, we observed that the shape retains at least up to $t = 40$.

At $t = 0$, the square amplitude and the phase of the matrix elements $\psi_Q(x, t)$ shown in panels (a) of Figure 3 and Figure 4 are identical to those of Figure 10 and 11 for $c = 0.05$ in Ref. [30], respectively. However, it follows from the phase field of the elliptic soliton solution that the time evolution of the quantum double dark-soliton is different from that of the travelling wave solution. The phase of the travelling wave solution is not shifted toward the negative direction in the time evolution. Thus, the time evolution of the quantum dark-solitons that we have constructed is slightly different from that of the elliptic soliton solution.

3.1.2. Quantum dark-soliton positions located at $X_1 = X_2 = 0$ initially By putting the quantum soliton positions X_1 and X_2 at the same position, the resultant profiles of the density and square amplitude are plotted in Figure 5 and 6, respectively. For both cases, the notches seem to repel each other in evolution.

For the density and the square amplitude, the quantum soliton with two overlapping positions has different properties from those of the quantum soliton state in Equation (6) where $X_1 = \frac{L}{4}$ and $X_2 = \frac{3L}{4}$. For the density profile case, we observed the notches in Figure 5 are deeper than those in Figure 2. For the square amplitude case, the bottoms of the notches increase in the time evolution: the bottoms of the notches are

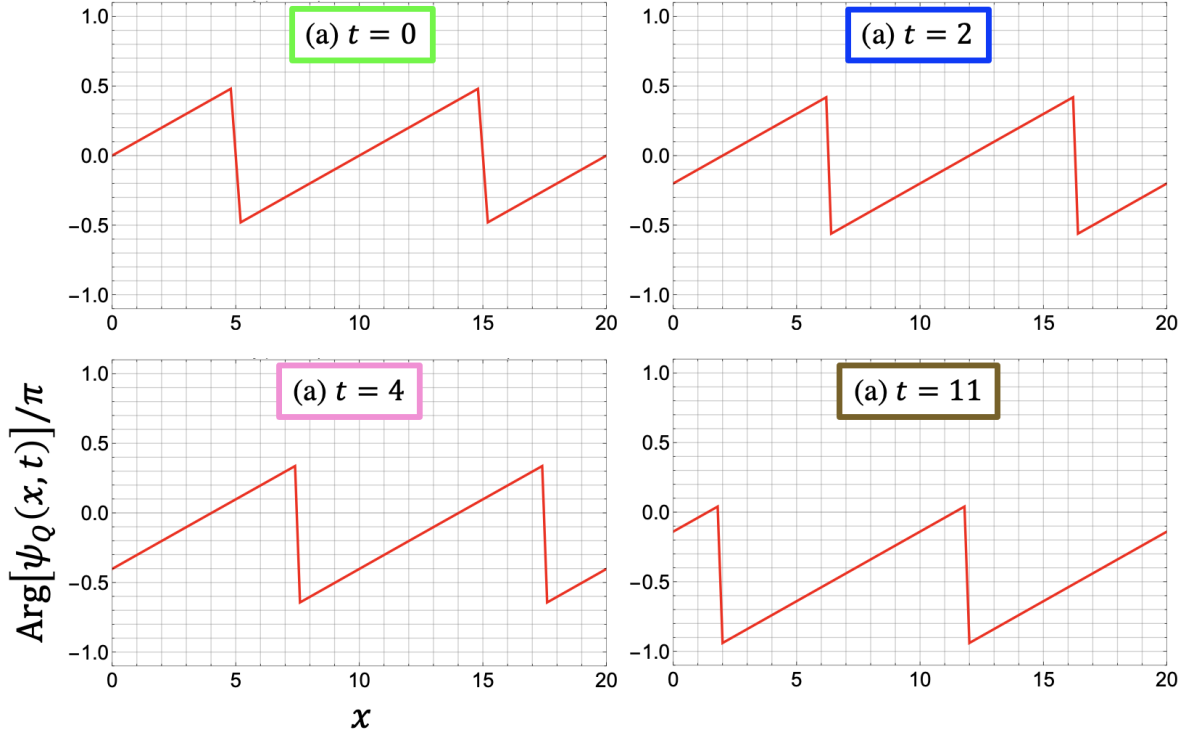


Figure 4. (Color online) Snapshots of the time evolution of the phase profile of the matrix elements $\psi_Q(x, t)$ at $t = 0, 2, 4, 11$, for $N = L = 20$, $X_1 = \frac{L}{4}$, $X_2 = \frac{3L}{4}$, and $c = 0.05$.

not close to zero any longer at $t = 11$ in Figure 6. Thus, for the quantum soliton with two overlapping positions the difference between the density profile and the square amplitude is smaller than Figure 2 and Figure 3.

Figure 7 shows the time evolution of the phase profile for the quantum soliton with two overlapping positions. For each panel, the phase profile satisfies the boundary conditions with nonzero winding numbers: $\text{Arg}[\psi_Q(x + L, t)] = \text{Arg}[\psi_Q(x, t)] + 2\pi J$ with the winding number $J \in \mathbb{Z}$. At $t = 0$, the winding number of the phase was given by $J = 2$, while it suddenly changed to $J = 1$ at $t = 0.05$. After the change of the winding number, the phase profile became smoother in shape gradually in time evolution. Furthermore Figure 7 shows that the whole phase is shifted toward the negative direction in time evolution. It is also the case in Figure 4 representing the phase profile where the soliton positions are different and put in the same distance.

The boundary conditions for the phase profile in the form of Equation (18) depends on the quantum dark-soliton state. However, the time evolution of the quantum state does not depend on the boundary conditions on the classical solutions. Since we evaluate the time evolution of the quantum dark-soliton state exactly, the sudden change of the winding number may occur for the quantum dark-soliton state.

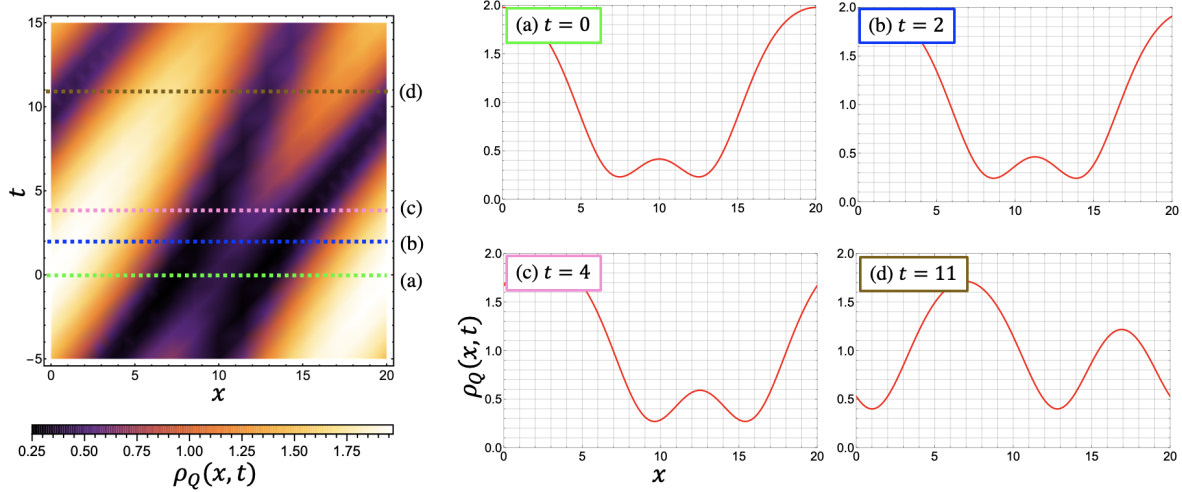


Figure 5. (Color online) Time evolution of the density profile $\rho_Q(x, t)$ (left panel) and its snapshots at $t = 0, 2, 4, 11$ (right panel) for $N = L = 20, X_1 = X_2 = 0$, and $c = 0.05$. Panel (a) shows the density profile at $t = 0$, which corresponds to the green dotted line in the left panel of the density plot. Panels (b), (c), and (d) shows the density profile at $t = 2, 4, 11$, which correspond to the blue, pink, and ochre dotted lines in the left panel of the density plot, respectively. The frames of the legends of panels (a), (b), (c), and (d) correspond to the green, blue, pink, and ochre colors, respectively.

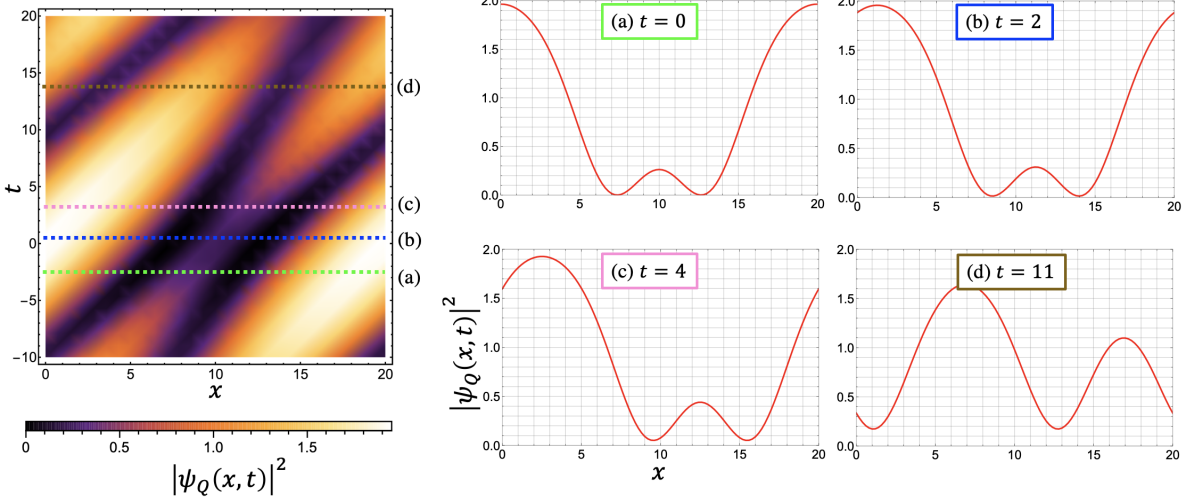


Figure 6. (Color online) Time evolution of the square amplitude of the matrix elements $\psi_Q(x, t)$ for $N = L = 20, X_1 = X_2 = 0$, and $c = 0.05$. Panel (a) shows the density profile at $t = 0$, which corresponds to the green dotted line in the left panel of the density plot. Panels (b), (c), and (d) shows the density profile at $t = 2, 4, 11$, which correspond to the blue, pink, and ochre dotted lines in the left panel of the density plot, respectively. The frames of the legends of panels (a), (b), (c), and (d) correspond to the green, blue, pink, and ochre colors, respectively.

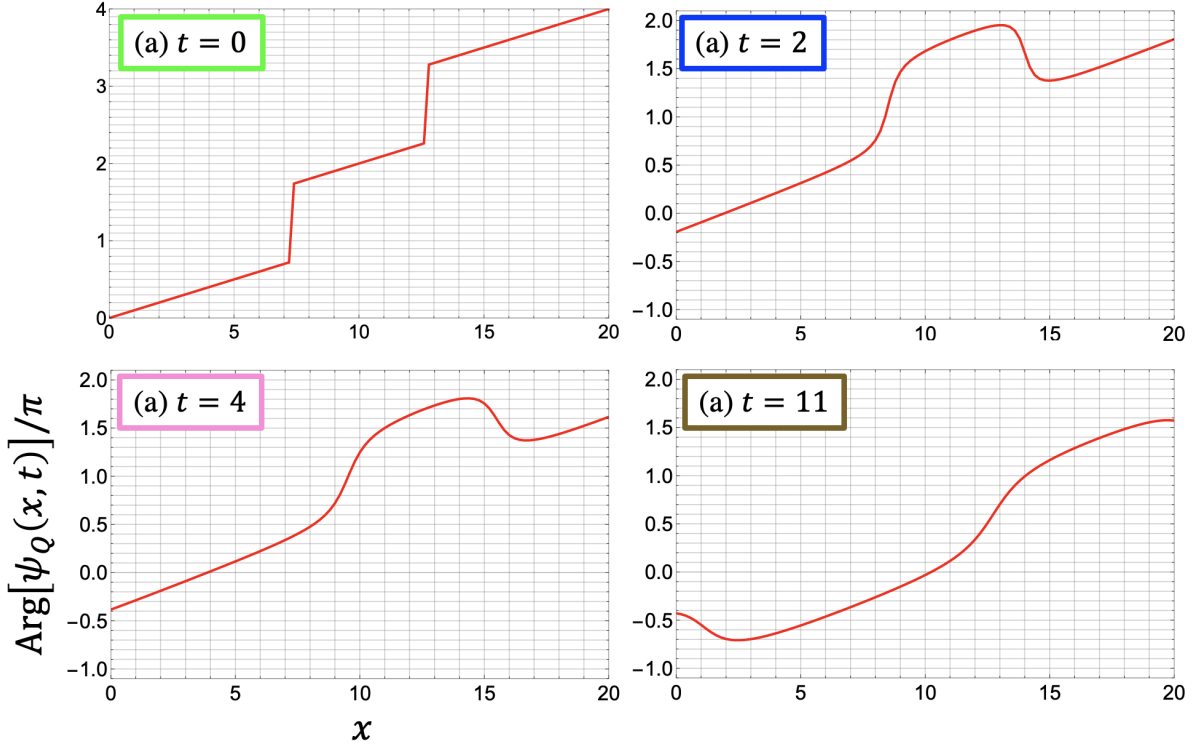


Figure 7. (Color online) The snapshots of the time evolution of the phase profile of the matrix elements $\psi_Q(x, t)$ at $t = 0, 2, 4, 11$ for $N = L = 20$, $X_1 = X_2 = 0$, and $c = 0.05$.

3.2. Time evolution of quantum double dark-soliton state with the Gaussian weights

Let us consider the Gaussian superposition of the excited states consisting of two particle-hole excitations which are determined by a pair of holes $\mathbf{p} = \{p_1, p_2\}$ in the set \mathbf{P} :

$$|X_1, X_2, N\rangle_G = \frac{1}{\sqrt{\mathcal{N}}} \sum_{\{p_1, p_2\} \in \mathbf{P}} G_{P_0}(p_1) G_{P'_0}(p_2) e^{i(p_1 X_1 + p_2 X_2)} |p_1, p_2, N\rangle. \quad (21)$$

Here, \mathcal{N} is a normalization factor and the set \mathbf{P} is the same as given in section 2.3. The Gaussian function is given by

$$G_P(q) = \exp \left[-\frac{(q - P)^2}{4\sigma^2} \right] \quad (22)$$

with two Gaussian parameters (P, σ) [15]. The parameters P and σ are determined by the target soliton depth d and density $n = N/L$;

$$P(d) = 2n \left\{ \frac{\pi}{2} - \left[\sqrt{\frac{d}{n}} \left(1 - \frac{d}{n} \right)} + \arcsin \left(\sqrt{\frac{d}{n}} \right) \right] \right\}, \quad (23)$$

$$\sigma^2 = \frac{4}{3} n \sqrt{nc} \left(1 - \frac{d}{n} \right)^{\frac{3}{2}}. \quad (24)$$

The target soliton depth d is expressed with the dark soliton solution to the GP equation moving with speed v in the thermodynamic limit $\phi_P^\infty(x)$ [15]:

$$\sqrt{d} = |\phi_P^\infty(x = 0)| = \sqrt{n} \left| \frac{v}{v_{c,\infty}} \right|. \quad (25)$$

Here $|\phi_P^\infty(x = 0)|$ denotes the square root of the local density at the origin, i.e., at the position of a notch, in the thermodynamic limit, and $v_{c,\infty}$ is called the critical velocity.

The density profile and the square amplitude profile of the matrix element evolve in time by applying the time-dependent field operator, as we have done in §3.1. By assigning target soliton depths to the two notches respectively, we have constructed a quantum double dark-soliton state such that its density profile has two distinct notches with different depths. In Figures 8, 9, 10, 11 we set the target soliton depths d for the Gaussian weights as 0.6 and 0. The Gaussian parameters are given by $(P_0, \sigma) = (0.124027\pi, 0.106667)$ and $(P'_0, \sigma') = (\pi, 0.421637)$, which are calculated by Equations 23 and 24.

Figure 8 shows the time evolution of the density profile of the quantum state constructed with the Gaussian weights for $c = 0.05$. We have constructed the double dark-solitons of distinct narrow notches with different depths. Note that different depths of dark solitons give different speeds in the same direction. We thus observed the scattering of two notches in the quantum double dark-soliton state, which has a characteristic property in soliton-soliton collisions [39]. As the two dark-solitons approached, they moved along approximately straight line trajectories with different constant velocities. The collision occurred around at $t = 11$ (see panel (c), which corresponds to the pink dotted line in the left panel of Figure 8). After the collision, each of the dark solitons travelled with the same speed before the collision. We confirmed the phase shift after the collision.

Let us investigate the phase shift more explicitly. By applying the Galilean transformation, that is, moving with the coordinate of the left-side quantum dark-soliton in Figure 8, we clearly confirm the phase shift after the collision as shown in Figure 9. The position of the deeper soliton is shifted from $x = 5$ to $x = 2.2$ as shown in panel (d) of Figure 9. The shift corresponds to the phase shift due to the collision of the two dark-solitons.

Figure 10 shows the time evolution of the square amplitude of the matrix element of the field operator with the Gaussian weights for $c = 0.05$. The quantum state is the same as that of Figure 8. We have constructed the double dark-solitons of distinct narrow notches with different depths as well as in the density profile. We observe the scattering of two notches in the quantum double dark-soliton state. As the two dark-solitons approached, they moved along approximately straight line trajectories with different constant velocities, as shown in Figure 10. The collision occurred around at $t = 11$ (see panel (c), which corresponds to the pink dotted line in the left panel of Figure 10). After the collision, each of the dark solitons travelled with the same speed before the collision. We observed at least approximately the same phase shift as shown in Figure 8.

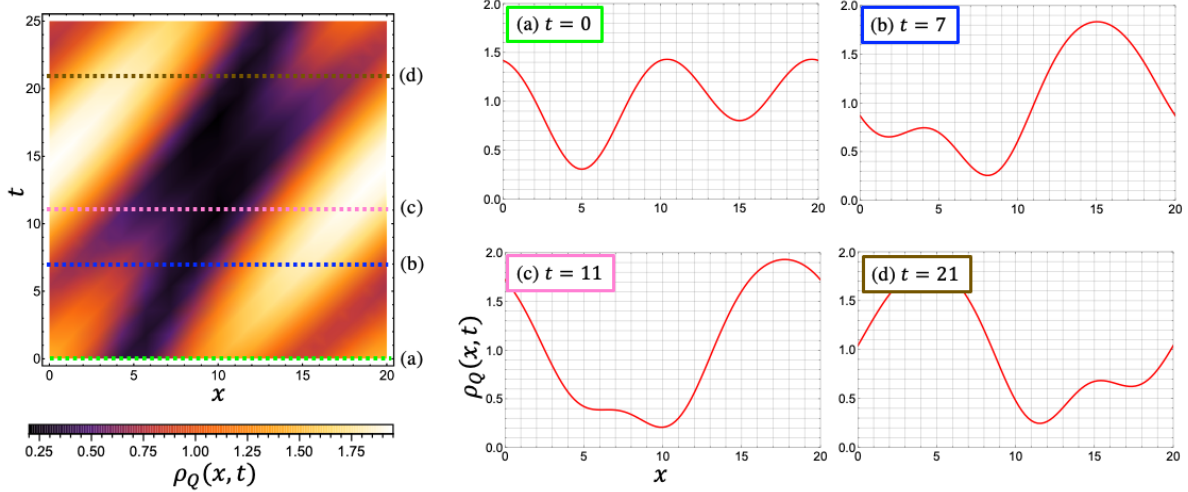


Figure 8. (Color online) Time evolution of the density profile with the Gaussian weights for $N = L = 20$, $X_1 = \frac{L}{4}$, $X_2 = \frac{3L}{4}$, and $c = 0.05$. Panels (a), (b), (c), and (d) shows the density profile at $t = 0, 7, 11, 21$, which correspond to the green, blue, pink, and ochre dotted lines in the left panel of the density plot, respectively. The frames of the legends of panels (a), (b), (c), and (d) correspond to the green, blue, pink, and ochre colors, respectively.

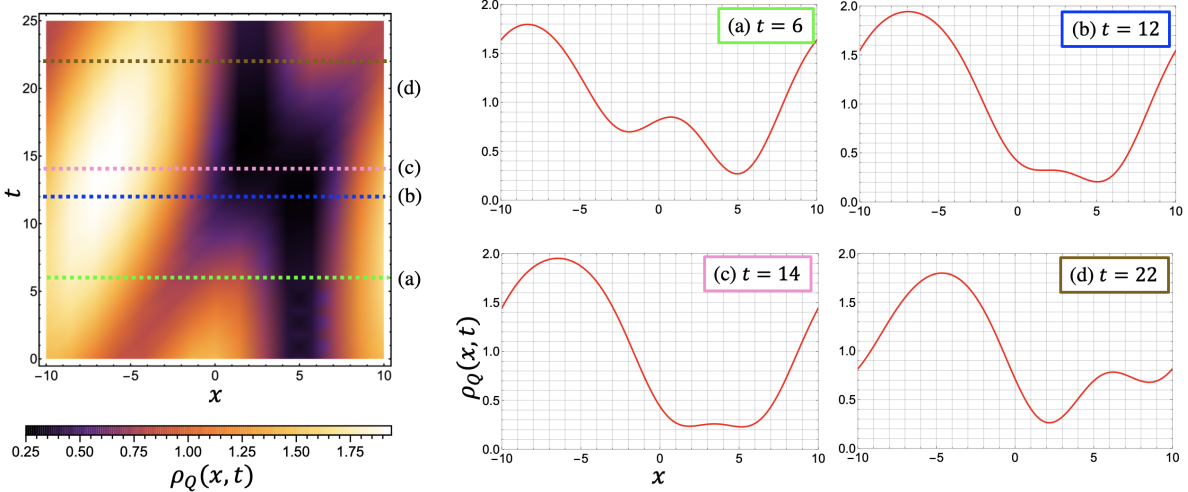


Figure 9. (Color online) Time evolution of the density profile with the Gaussian weights (left panel) and its snapshots at $t = 6, 12, 14, 22$ for $N = L = 20$, $X_1 = -L/4$, $X_2 = L/4$, and $c = 0.05$, performed by the Galilean transformation. Panels (a), (b), (c), and (d) show the density profile at $t = 6, 12, 14, 22$, which correspond to the green, blue, pink, and ochre dotted lines in the left panel of the density plot, respectively. The frames of the legends of panels (a), (b), (c), and (d) correspond to the green, blue, pink, and ochre colors, respectively.

We now show that the winding number is changed during the scattering. Figure 11 shows the time evolution of the phase profile. In each panel, the phase profile satisfies the boundary conditions: $\text{Arg}[\phi_Q(x + L, t)] = \text{Arg}[\phi_Q(x, t)] + 2\pi J$ with the winding number J . At the beginning, $t = 0$, when the quantum solitons were put in the same

distance the winding number is $J = 1$. When the two quantum dark-solitons were close enough, the winding number was suddenly changed to $J = 0$ approximately at $t = 11$, as shown in panel (c) of Figure 11. After the collision, the winding number was recovered: the winding number at $t = 21$ became $J = 1$, as shown in panel (d) of Figure 11.

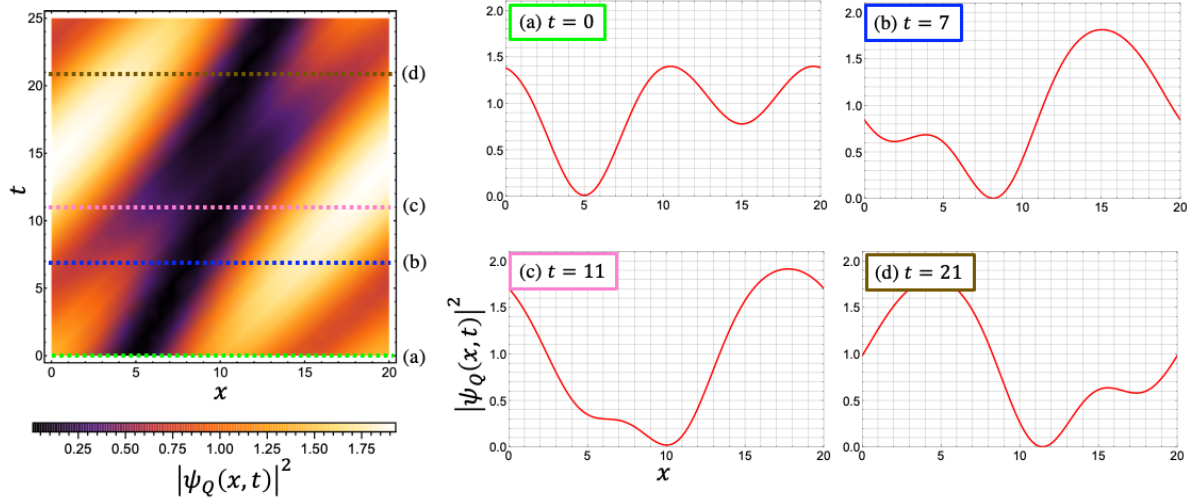


Figure 10. (Color online) Time evolution of the square amplitude with Gaussian weights and its snapshots at $t = 0, 7, 11, 21$ for $N = L = 20$, $X_1 = \frac{L}{4}$, $X_2 = \frac{3L}{4}$, and $c = 0.05$. Panels (a), (b), (c), and (d) shows the density profile at $t = 0, 12, 14, 22$, which correspond to the green, blue, pink, and ocher dotted lines in the left panel of the density plot, respectively. The frames of the legends of panels (a), (b), (c), and (d) correspond to the green, blue, pink, and ocher colors, respectively.

The Gaussian weights lead to the different depths for quantum double dark-solitons[30]. This gives the notches of the quantum double dark-soliton state different speeds, and we observe the scattering of two notches in the quantum double dark-soliton state exactly. We suggest that the winding number of a quantum double dark-soliton state may change when the two notches approach.

4. Finite-Size Scaling of BEC

4.1. Motivation to study the quasi-BEC in 1D

In 1D systems quantum fluctuations play a key role and often give subtle and nontrivial effects. It is known that BEC occurs even for bosons with repulsive interactions due to the quantum statistical effect among identical particles [40]. In fact, the existence of BEC has been proven rigorously for interacting bosons confined in dimensions greater than one [41]. In 1D case there is no BEC for bosons with repulsive interactions due to strong quantum fluctuations if we take the standard thermodynamic limit with fixed coupling constant [42]. On the other hand, if the coupling constant is very weak, we may expect that even the 1D bosons with a large but finite number of particles undergo

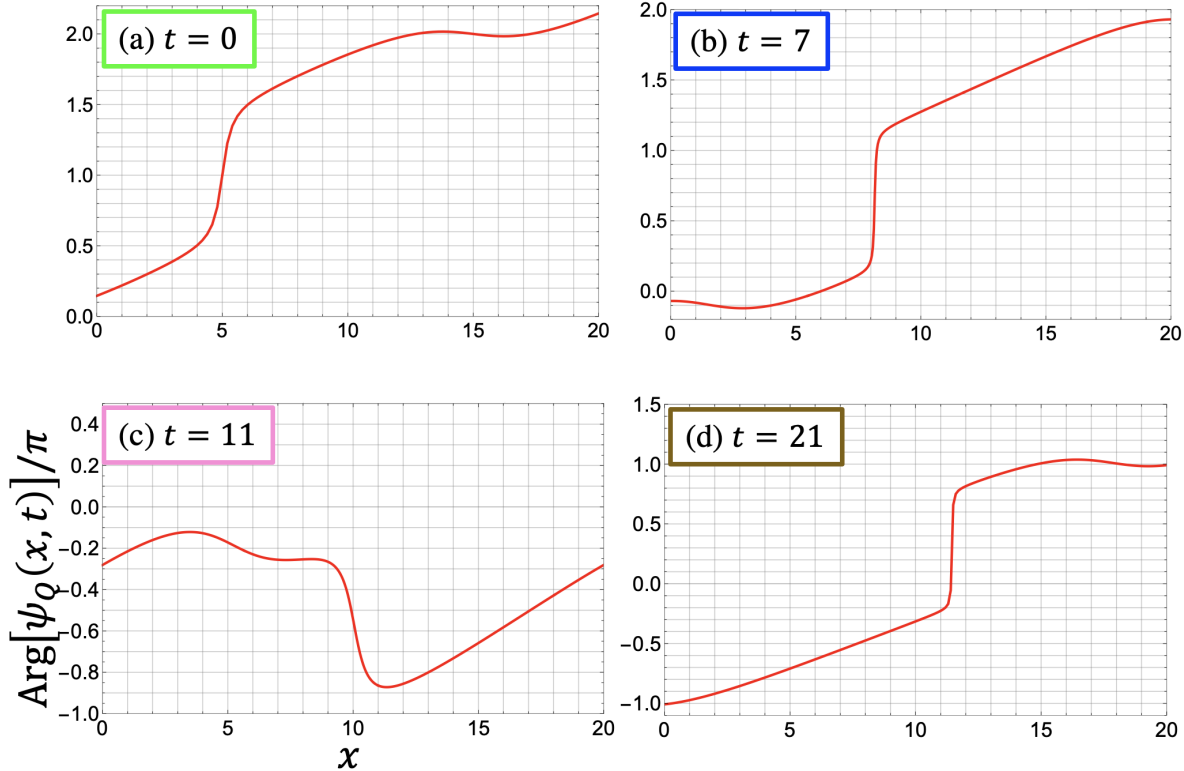


Figure 11. (Color online) The snapshots of the time evolution of the phase profile with Gaussian weights at $t = 0, 7, 11, 21$ for $N = L = 20$, $X_1 = \frac{L}{4}$, $X_2 = \frac{3L}{4}$, and $c = 0.05$.

a quasi-condensation in which “a macroscopic number of particles occupy a single one-particle state” [40].

However, it has not been shown explicitly how such a quasi-condensation occurs in interacting bosons in one dimension. Furthermore, it is nontrivial to expect it for the 1D Bose gas that is solvable by the Bethe ansatz. No pair of particles can have the same quasi-momentum in common for a Bethe-ansatz solution. Here we call the 1D system of bosons interacting with repulsive delta-function potentials the 1D Bose gas. For the impenetrable 1D Bose gas where the coupling constant is taken to infinity, condensate fractions are analytically and numerically studied [43], while in the weak coupling case it is nontrivial to evaluate the fractions in the 1D Bose gas.

4.2. Onsager-Penrose criterion of BEC

Let us review the definition of BEC through the one-particle reduced density matrix for a quantum system [40, 44]. We assume that the number of particles N is very large but finite. At zero temperature, the density matrix is given by $\hat{\rho} = |\lambda\rangle\langle\lambda|$, where $|\lambda\rangle$ denotes the ground state of the quantum system. We define the one-particle reduced density matrix by the partial trace of the density matrix with respect to other degrees of freedom: $\hat{\rho}_1 = N\text{tr}_{23\dots N}\hat{\rho}$. This matrix is positive definite and hence it is diagonalized

as

$$\hat{\rho}_1 = N_0 |\Psi_0\rangle\langle\Psi_0| + N_1 |\Psi_1\rangle\langle\Psi_1| + \dots \quad (26)$$

Here we put eigenvalues N_j in descending order: $N_0 \geq N_1 \geq N_2 \geq \dots > 0$. The sum of all the eigenvalues is given by the number of particles: $\sum_j N_j = N$. Here we recall $\text{tr}_1 \hat{\rho}_1 = N$ due to the normalization: $\text{tr}_{123\dots N} \hat{\rho} = 1$. Let us denote by n_0 the ratio of the largest eigenvalue N_0 to particle number N :

$$n_0 := N_0/N. \quad (27)$$

The criterion of BEC due to Penrose and Onsager [44] is given as follows: If the largest eigenvalue N_0 is of order N , i.e. the ratio n_0 is nonzero and finite for large N , then we say that the system exhibits BEC, and we call n_0 the condensate fraction. Here we also define fractions n_j by $n_j = N_j/N$ for $j = 1, 2, \dots$

4.3. Saturation rate

c	0.01	1	100
1p1h	0.999984	0.971538	0.693620
2p2h	1.59454×10^{-5}	0.0280102	0.289056
n_{sat}	1.00000	0.999548	0.982676

Table 1. (Color online) Fraction n_{sat} of the reduced density operator at the origin, $\rho_1(0, 0)$, to the density n , evaluated by taking the sum over a large number of eigenstates $|\mu\rangle$ with one particle and one hole (1p1h) or with two particles and two holes (2p2h) for $N = L = 50$ ($n = 1$): $n_{\text{sat}} = \left(\sum_{\mu}^{1p1h} + \sum_{\mu}^{2p2h} \right) |\langle \mu | \hat{\psi}(0) | \lambda \rangle|^2 / n$.

Numerically we calculate correlation function (15) by taking the sum over a large number of eigenstates with one particle and one hole (1p1h) and those with two particles and two holes (2p2h). In order to confirm the validity of the restricted sum, we have estimated the ratio of the one-particle reduced density operator at the origin to density n , $\rho_1(0, 0)/n$, through the form factor expansion (15) for the excitations with 1p1h or 2p2h. We express it by n_{sat} . The estimates of n_{sat} are listed in Table 1. The graph of n_{sat} approaches 1 for small coupling constant c , while it is larger than 0.98 for any value of c in the case of $N = 50$.

4.4. Evaluation of the one-particle reduced density matrix

For the LL model, the eigenfunctions of the one-particle reduced density matrix are given by plane waves for any nonzero and finite value of c . It is a consequence of the translational invariance of the Hamiltonian of the LL model. We thus have

$$\rho_1(x, y) = \frac{N_0}{L} + \sum_{j=1}^{\infty} \frac{2N_j}{L} \cos [2\pi j(x - y)/L]. \quad (28)$$

The eigenvalues of the one-particle reduced density matrix, N_j , are expressed in terms of the form factor expansion. We consider the sum over all the form factors between the ground state, $|\lambda\rangle$, and such eigenstates, $|\mu\rangle$, that have a given momentum P_j as

$$N_j = L \sum_{\mu: P_\mu = P_j} |\langle \mu | \hat{\psi}(0) | \lambda \rangle|^2. \quad (29)$$

In the LL model we have $P_j := (2\pi/L)j$.

Solving the Bethe ansatz equations for a large number of eigenstates we observe numerically that eigenvalues N_j are given in decreasing order with respect to integer j : $N_0 > N_1 > N_2 > \dots$. It thus follows that condensate fraction which corresponds to the largest eigenvalue of the one-particle reduced density matrix $\hat{\rho}_1$ is indeed given by $n_0 = N_0/N$, where N_0 has been defined by sum (29) over all eigenstates with zero momentum.

4.5. Condensate fraction in the weak coupling regime

The estimates of condensate fraction n_0 are plotted against coupling constant c in the upper panel of Figure 12 over a wide range of c such as from $c = 10^{-3}$ to $c = 10^3$ for different values of particle number N such as $N = 4, 10, \dots, 400$. For each N , condensate fraction n_0 becomes 1.0 for small c such as $c < 0.01$, while it decreases with respect to c and approaches an asymptotic value in the large c region such as $c > 100$ or 1000. The asymptotic values depend on particle number N for $N = 4, 10, \dots, 400$, and they are consistent with the numerical estimates of occupation numbers for the impenetrable 1D Bose gas (see eq. (56) of Ref. [43]). In the lower panel of Figure 12, we plot fractions n_j for $j = 0, 1$ and 2 against coupling constant c from $c = 10^{-3}$ to $c = 10^3$ with $N = 20$. The asymptotic values of n_j for large c (i.e. $c = 1000$) are consistent with the numerical estimates for the impenetrable 1D Bose gas (for n_1 and n_2 , see eqs. (57) and (58) of Ref. [43], respectively).

We observe that condensate fraction n_0 decreases as particle number N increases where density $n = N/L$ is fixed. It is the case for $c < 0.1$ in the upper panel of Figure 12. Condensate fraction n_0 decreases as N increases even for small c such as $c = 0.01$, as shown in Figure 13. Thus, it is necessary for coupling constant c to decrease with respect to N so that condensate fraction n_0 remains constant as N increases with fixed density n .

4.6. Exact finite-size scaling

We now show the finite-size scaling of condensate fraction n_0 . In Figure 14 each contour line gives the graph of interaction parameter γ as a function of the inverse of particle number N for a fixed value of condensate fraction n_0 . They are plotted for various values of n_0 from $n_0 = 0.6$ to 0.99, and are obtained by solving the Bethe-ansatz equations numerically.

For different values of density such as $n = 1, 2$ and 5, we have plotted contour lines with fixed values of condensate fraction n_0 in the plane of interaction parameter γ

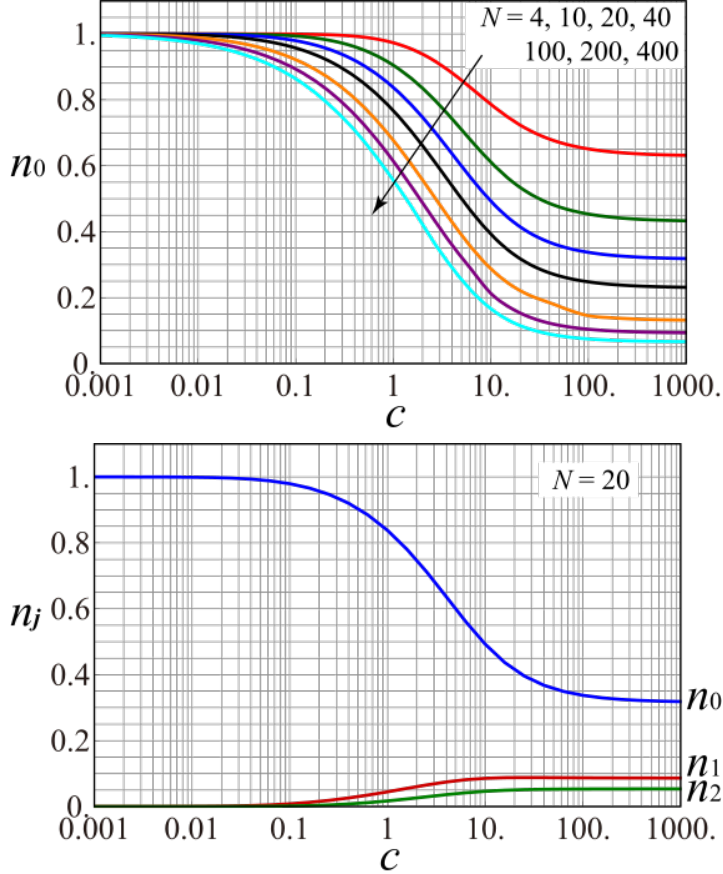


Figure 12. (Color online) Dependence of fractions n_j on coupling constant c . In the upper panel: condensate fraction n_0 is plotted against coupling constant c for $N = 4, 10, 20, 40, 100, 200$ and 400 , from the top to the bottom, in red, green, blue, black, orange, purple and cyan lines, respectively. In the lower panel: condensate fraction n_0 , fractions n_1 and n_2 are shown against c from the top to the bottom in blue, red and green lines, respectively, for $N = 20$. We recall $n = N/L = 1$.

versus inverse particle number $1/N$. We have observed that the contours with the same condensate fraction n_0 but for the different densities coincided with each other in the γ versus $1/N$ plane. Furthermore, they are well approximated by

$$\gamma = A/N^\eta. \quad (30)$$

Thus, condensate fraction n_0 is constant as particle number N becomes very large if interaction parameter γ is given by the power of particle number N as in eq. (30).

Applying the finite-size scaling arguments, we suggest from eq. (30) that condensation fraction n_0 is given by a scaling function $\phi(\cdot)$ of a single variable γN^η : $n_0 = \phi(\gamma N^\eta)$. Here we recall the coincidence of contours for the different values of density n in Figure 14. We thus observe that exponent η and amplitude A of eq. (30) are determined only by condensate fraction n_0 and are independent of density n .

Let us consider amplitude A as a function of n_0 . We denote it by $A = f(n_0)$. Then, the scaling function $\phi(\cdot)$ is given by the inverse function: $n_0 = f^{-1}(A)$. In Figure 4.7,

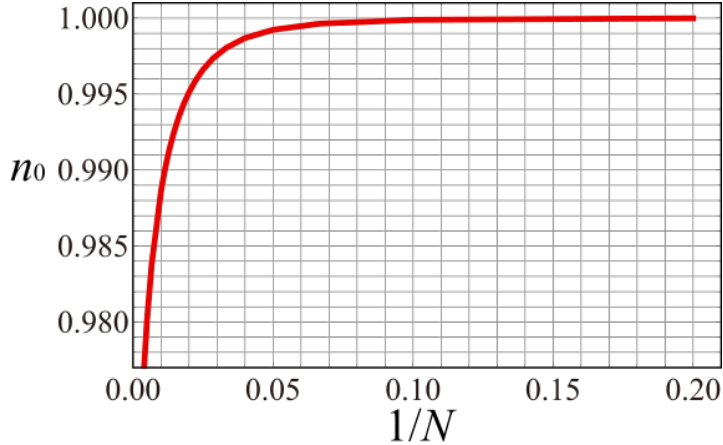


Figure 13. (Color online) Condensate fraction n_0 as a function of $1/N$ for $c = 0.01$. Here $n = N/L = 1.0$.

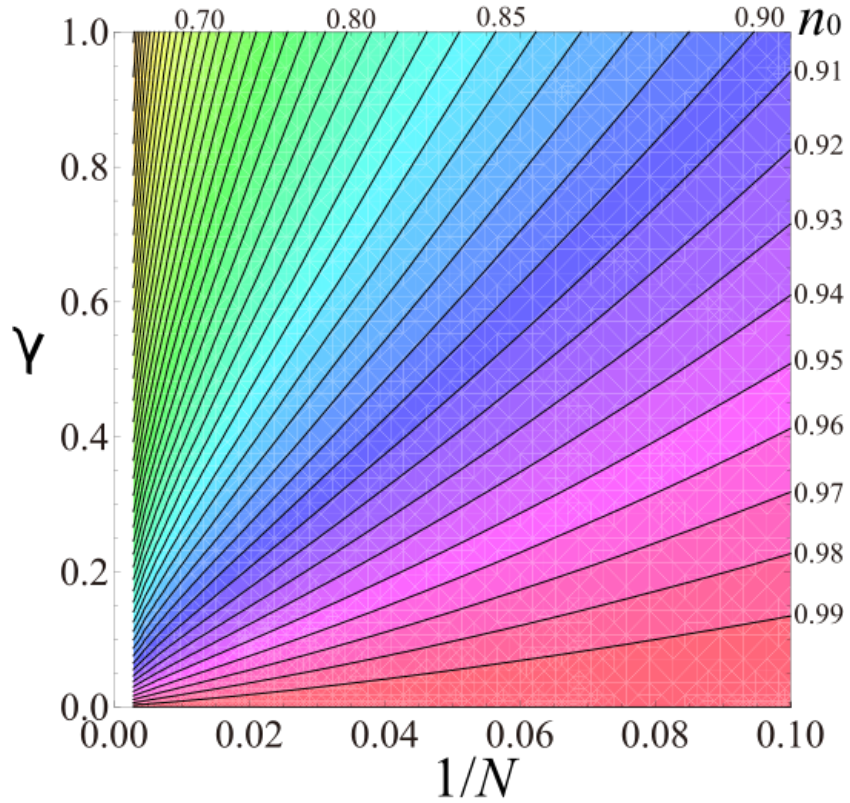


Figure 14. (Color online) Contours of condensate fraction n_0 are plotted for various values of n_0 in the γ versus $1/N$ plane. Each contour is approximated by (30): γ as a function of $1/N$.

exponent η increases with respect to n_0 , and amplitude A decreases monotonically with respect to n_0 .

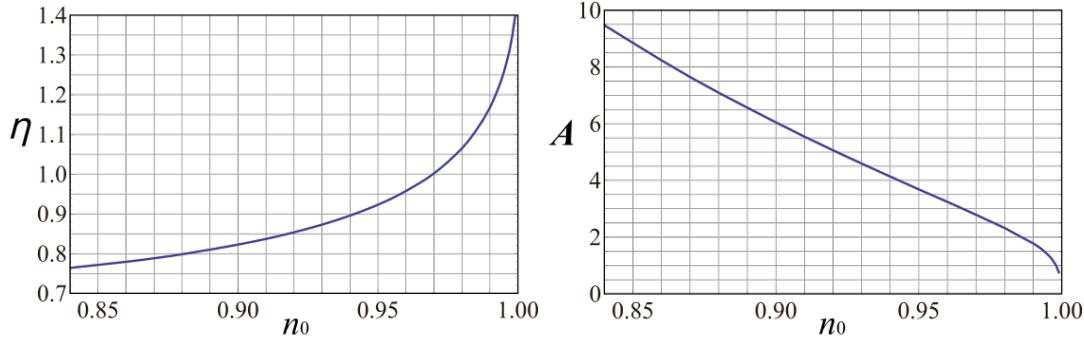


Figure 15. (Color online) Exponent η and amplitude A as functions of condensate fraction n_0 .

4.7. Quasi-BEC according to the Onsager-Penrose criterion

It follows from (30) that BEC does not occur in the 1D Bose gas if we fix parameter γ and density n as system size L goes to infinity. However, if γ is small enough so that it satisfies eq. (30) for a given value of condensate fraction n_0 , the 1D Bose gas shows BEC from the viewpoint of the Penrose and Onsager criterion. We suggest that if condensate fraction n_0 of a quantum state is nonzero and finite for large N , the mean-field approximation is valid for the quantum state. For instance, there exist such quantum states that correspond to classical dark-solitons of the GP equation [12], if parameter γ is small enough so that it satisfies (30).

4.8. Various limiting procedures

With the scaling behavior (30) we derive various ways of the thermodynamic limit such that condensate fraction n_0 is constant. For instance, we consider the case of a finite particle number, $N = N_f$. Choosing a value of n_0 , we determine γ by eq. (30) as $\gamma = A(n_0)/N_f^{\eta(n_0)}$. Then, the 1D Bose gas with $N = N_f$ has the same condensate fraction n_0 for any large value of L if coupling constant c is given by $c = A(n_0)N_f^{1-\eta}/L$. Let us set $\eta = 1$ and $N_f = 10$, for simplicity. We have $n_0 = 0.97$ in Figure 4.7, and $\gamma = 0.3$ at $1/N = 0.1$ in the contour of $n_0 = 0.97$ in Figure 14. By assuming $n = 1$, it corresponds to the case of $L = 10$ and $c = 0.3$, and we have $A = cL = 3$, which is consistent with Figure 4.7. Therefore, the 1D Bose gas with $N_f = 10$ has $n_0 = 0.97$ for any large L if c is given by $c = 0.3/L$. Moreover, we may consider other types of thermodynamic limits. When density n is proportional to a power of L as L^α , condensate fraction n_0 is constant as L goes to infinity if we set $c \propto L^{(1-\eta)(1+\alpha)-1}$.

The scaling law (30) and the estimates of condensate fraction in the present paper should be useful for estimating conditions in experiments of trapped cold atomic gases in one dimension [45]. For instance, we suggest from Figure 1 that BEC may appear in 1D systems with a small number of bosons such as $N = 20$ or 40 for $c = 1$ or 10 .

5. Concluding remarks

In the first part, we have shown that the density profile and the square amplitude evolved in time differently, in particular, for the equal weight case. In the former the notches were filled progressively, while the amplitude of the latter decreased gradually. Furthermore, the Gaussian weights led to the different depths for quantum double dark-solitons[30]. This gave the two notches of the quantum double dark-soliton the different speeds, and we observed the scattering of the two notches in the quantum double dark-soliton state exactly. Interestingly, the winding number of the quantum double dark-soliton state has changed when the two notches approach.

In the second part, we exactly calculated the condensate fraction of the 1D Bose gas with repulsive interaction by the form factor expansion. We have shown the finite-size scaling behavior such that condensate fraction n_0 is given by a scaling function of interaction parameter γ times some power of particle number N : $n_0 = \phi(\gamma N^\eta)$. Consequently, if parameter γ decrease as $\gamma = A/N^\eta$, condensate fraction n_0 remains nonzero and constant as particle number N becomes very large. By modifying the thermodynamic limit, the 1D Bose gas shows BEC from the viewpoint of the Penrose-Onsager criterion.

6. Acknowledgements

The present research is partially supported by Grant-in-Aid for Scientific Research No. 21K03398. K. K. is supported by the Japan Science Technology Agency (CREST Grant Number JPMJCR 19T4).

References

- [1] Görlitz A, Vogels J M, Leanhardt A E, Raman C, Gustavson T L, Abo-Shaeer J R, Chikkatur A P, Gupta S, Inouye S, Rosenband T and Ketterle W 2001 *Phys. Rev. Lett.* **87**(13) 130402 URL <https://link.aps.org/doi/10.1103/PhysRevLett.87.130402>
- [2] Greiner M, Bloch I, Mandel O, Hänsch T W and Esslinger T 2001 *Phys. Rev. Lett.* **87**(16) 160405 URL <https://link.aps.org/doi/10.1103/PhysRevLett.87.160405>
- [3] Kinoshita T, Wenger T and Weiss D S 2004 *Science* **305** 1125–1128 URL <https://www.science.org/doi/abs/10.1126/science.1100700>
- [4] Weller A, Ronzheimer J P, Gross C, Esteve J, Oberthaler M K, Frantzeskakis D J, Theocharis G and Kevrekidis P G 2008 *Phys. Rev. Lett.* **101**(13) 130401 URL <https://link.aps.org/doi/10.1103/PhysRevLett.101.130401>
- [5] Becker C, Stellmer S, Soltan-Panahi P, Dörscher S, Baumert M, Richter E M, Kronjäger J, Bongs K and Sengstock K 2008 *Nature Physics* **4** 496–501
- [6] Burger S, Bongs K, Dettmer S, Ertmer W, Sengstock K, Sanpera A, Shlyapnikov G V and Lewenstein M 1999 *Phys. Rev. Lett.* **83**(25) 5198–5201 URL <https://link.aps.org/doi/10.1103/PhysRevLett.83.5198>
- [7] Katsimiga G, Mistakidis S, Koutentakis G, Kevrekidis P and Schmelcher P 2017 *New Journal of Physics* **19** 123012
- [8] Delande D and Sacha K 2014 *Phys. Rev. Lett.* **112**(4) 040402 URL <https://link.aps.org/doi/10.1103/PhysRevLett.112.040402>

- [9] Lieb E H and Liniger W 1963 *Phys. Rev.* **130**(4) 1605–1616 URL <https://link.aps.org/doi/10.1103/PhysRev.130.1605>
- [10] Lieb E H 1963 *Phys. Rev.* **130**(4) 1616–1624 URL <https://link.aps.org/doi/10.1103/PhysRev.130.1616>
- [11] Pitaevskii L and Stringari S 2003 *Bose-einstein condensation* oxford university press
- [12] Sato J, Kanamoto R, Kaminishi E and Deguchi T 2012 *Phys. Rev. Lett.* **108** 110401
- [13] Ishikawa M and Takayama H 1980 *Journal of the Physical Society of Japan* **49** 1242–1246 (*Preprint* <https://doi.org/10.1143/JPSJ.49.1242>) URL <https://doi.org/10.1143/JPSJ.49.1242>
- [14] Sato J, Kanamoto R, Kaminishi E and Deguchi T 2016 *New Journal of Physics* **18** 075008 URL <https://doi.org/10.1088%2F1367-2630%2F18%2F7%2F075008>
- [15] Kaminishi E, Mori T and Miyashita S 2020 *Journal of Physics B: Atomic, Molecular and Optical Physics* **53** 095302
- [16] Shamailov S S and Brand J 2019 *Phys. Rev. A* **99**(4) 043632 URL <https://link.aps.org/doi/10.1103/PhysRevA.99.043632>
- [17] Ishiguro Y, Sato J and Nishinari K 2022 Multi-quantum dark solitons in one-dimensional bose gas (*Preprint* [arXiv:2203.01211](https://arxiv.org/abs/2203.01211))
- [18] Syrwid A and Sacha K 2015 *Phys. Rev. A* **92**(3) 032110 URL <https://link.aps.org/doi/10.1103/PhysRevA.92.032110>
- [19] Syrwid A 2021 *Journal of Physics B: Atomic, Molecular and Optical Physics* **54** 103001 URL <https://doi.org/10.1088/1361-6455/abd37f>
- [20] Golletz W, Górecki W, Ołdziejewski R and Pawłowski K 2020 *Phys. Rev. Research* **2**(3) 033368 URL <https://link.aps.org/doi/10.1103/PhysRevResearch.2.033368>
- [21] Sato J, Kanamoto R, Kaminishi E and Deguchi T 2012 *Phys. Rev. Lett.* **108**(11) 110401 URL <https://link.aps.org/doi/10.1103/PhysRevLett.108.110401>
- [22] Kopyciński J, Lebek M, Marciak M, Ołdziejewski R, Górecki W and Pawłowski K 2022 *SciPost Physics* **12** 023
- [23] Morera Navarro I, Guilleumas M, Mayol R and Mateo A M n 2018 *Phys. Rev. A* **98**(4) 043612 URL <https://link.aps.org/doi/10.1103/PhysRevA.98.043612>
- [24] Liang Z, Zhang Z and Liu W 2005 *Physical review letters* **94** 050402
- [25] Wang D S, Hu X H, Hu J and Liu W 2010 *Physical Review A* **81** 025604
- [26] Wen L, Li L, Li Z D, Song S W, Zhang X F and Liu W 2011 *The European Physical Journal D* **64** 473–478
- [27] Li L, Li Z, Malomed B A, Mihalache D and Liu W 2005 *Physical Review A* **72** 033611
- [28] Korepin V E, Bogoliubov N M and Izergin A G 1993 *Quantum Inverse Scattering Method and Correlation Functions* Cambridge Monographs on Mathematical Physics (Cambridge University Press)
- [29] Dorlas T C 1993 *Communications in mathematical physics* **154** 347–376
- [30] Kinjo K, Kaminishi E, Mori T, Sato J, Kanamoto R and Deguchi T 2022 *Universe* **8** 2
- [31] Gaudin M 1983 *La fonction d'onde de Bethe* vol 1 (Elsevier Masson)
- [32] Korepin V E 1982 *Communications in Mathematical Physics* **86** 391–418
- [33] Slavnov N A 1989 *Teoreticheskaya i Matematicheskaya Fizika* **79** 232–240
- [34] Caux J S, Calabrese P and Slavnov N A 2007 *Journal of Statistical Mechanics: Theory and Experiment* **2007** P01008–P01008 URL <https://doi.org/10.1088/1742-5468/2007/01/p01008>
- [35] Kojima T, Korepin V E and Slavnov N 1997 *Communications in mathematical physics* **188** 657–689
- [36] Slavnov N A 1990 *Theoretical and Mathematical Physics* **82** 273–282
- [37] Kanamoto R, Carr L D and Ueda M 2008 *Phys. Rev. Lett.* **100**(6) 060401 URL <https://link.aps.org/doi/10.1103/PhysRevLett.100.060401>
- [38] Kanamoto R, Carr L D and Ueda M 2009 *Phys. Rev. A* **79**(6) 063616 URL <https://link.aps.org/doi/10.1103/PhysRevA.79.063616>

- [39] Kaminishi E, Mori T and Ueda M 2019 Dynamics of the quanutm dark soliton the 74th Annual Meeting of the Physical Society of Japan
- [40] Leggett A J *et al.* 2006 *Quantum liquids: Bose condensation and Cooper pairing in condensed-matter systems* (Oxford university press)
- [41] Lieb E H and Seiringer R 2002 *Phys. Rev. Lett.* **88**(17) 170409 URL <https://link.aps.org/doi/10.1103/PhysRevLett.88.170409>
- [42] Pitaevskii L and Stringari S 1991 *Journal of low temperature physics* **85** 377–388
- [43] Forrester P J, Frankel N E, Garoni T M and Witte N S 2003 *Phys. Rev. A* **67**(4) 043607 URL <https://link.aps.org/doi/10.1103/PhysRevA.67.043607>
- [44] Penrose O and Onsager L 1956 *Phys. Rev.* **104**(3) 576–584 URL <https://link.aps.org/doi/10.1103/PhysRev.104.576>
- [45] Pitaevskii L and Stringari S 2003 *Bose-Einstein Condensation* International series of monographs on physics (Clarendon Press) ISBN 0 19 850719-4